# MODULATED STRUCTURES OF ADSORBED RARE GAS MONOLAYERS

Klaus Kern and George Comsa

Institut für Grenzflächenforschung und Vakuumphysik
Forschungszentrum Jülich, Postfach 1913, D-5170 Jülich, FRG

## ABSTRACT

The structure of rare gas adlayers is determined by the interplay between the mutual interaction of the rare gas atoms and the interaction of the rare gas atom with the substrate. Depending on the relative magnitude of these interactions different types of structures of the first monolayer appear: if the mutual interaction is dominant the rare gas adlayer is incommensurate with the substrate. When the interactions are of the same order, a large variety of phases (incommensurate -I-, commensurate -C-, higher order commensurate -HOC) appear depending on temperature, coverage and the relative structure of the substrate and the of the bulk rare gas crystal. By varying the temperature and/or the coverage a whole series of phases are visited from commensurate, over striped and hexagonal incommensurate, to hexagonal incommensurate rotated, which ends in a high order commensurate phase. In between there are both first and second order phase transitions. On the other hand, when the lock-in forces of the substrate dominate, all or a fraction of the adatoms will always lock into preferential adsorption sites and commensurate or high order commensurate phases, repsectively, are energetically favored with respect to true floating incommensurate structures.

## 1. INTRODUCTION

The investigation of physisorbed rare gas adlayers has proven to be a powerful tool in the understanding of elementary surface processes, such as adsorption and desorption, surface melting or wetting [1]. In addition,

*Phase Transitions in Surface Films 2*
Edited by H. Taub *et al.*, Plenum Press, New York, 1991

physisorption systems have acquired model character in the study of structural and dynamical properties of adsorbed layers and thin films [2], providing model systems of 2D phases and their mutual transitions.

In a simplified picture the structure of an adsorbed layer is governed by the competition between the lateral adatom-adatom interaction and the surface corrugation potential of the underlying substrate. On the one hand, the lateral interaction between the adatoms will tend to establish an adlayer structure determined by the natural adlayer interatomic distance, i.e. incommensurate with the substrate. On the other hand, the lateral variation of the substrate-adatom potential (corrugation) will try to force the adatoms to occupy energetically favoured adsorption sites, hence leading to a commensurate structure. In the case where the lateral adatom interaction and the corrugation of the adatom-substrate potential have about the same magnitude, the kind of adlayer structure (commensurate or incommensurate) will largely depend on the structures symmetries, and the ratio of the lattice constants as well as on the actual conditions, such as coverage, spreading pressure, and surface temperature. Varying these conditions, structural phase transitions between different commensurate and incommensurate phases may occur and complex phase diagrams are obtained as for instance in the case of physisorbed rare gases on graphite [3] and metal surfaces [2].

Moreover, enhanced fluctuation effects due to the reduced dimensionality add to the fascination of these delicate physical systems. While phase fluctuations dominate low-temperature behavior of 2D-phases, amplitude fluctuations dominate at higher temperatures when approaching the critical temperature. Indeed, phase fluctuations, in form of long-wavelength phonons, are responsible for the supression of a genuine long-range order in two-dimensional solids, at all temperatures $T > 0K$ . Amplitude fluctuations, which are always present and dominate at high enough temperatures, appear in 2D systems in the form of defects, in particular as dislocations in 2D solids. Such dislocations (often termed domain walls or solitons) result by adding or removing a half-infinite row of atoms from an otherwise perfect lattice. They play a central role in phase transitions of quasi two-dimensional systems, in the melting transition as well as in the registry-disregistry transition.

The dominance of fluctuations in lower-dimensional systems can also be understood by simple arguments. The order of a phase is thermodynamically determined by the free energy, i.e. by the competition between energy and entropy. In three-dimensional systems each atom has a large number of

nearest neighbors (12 in a fcc crystal), thus the energy term stabilizes an ordered state, local fluctuations being of minor importance. In one dimension, however, each atom has only two nearest neighbors. Here the entropy term dominates the energy term, and even very small local fluctuations destroy the order. In a close packed two-dimensional system each atom has six nearest neighbors and, depending on temperature, energy and entropy may be in balance. As amplitude fluctuations, i.e. topological defects, can be excited thermally, the two-dimensional systems seem to be ideally suited for studying defect-mediated phase transitions.

High resolution scattering of thermal He-atoms is a particularly appropriate tool for the study of rare gas layers on metal surfaces. This is not only because structural and dynamical information are both accessible in great detail, but in addition, due to the extreme sensitivity of the He scattering with respect to defects and impurities, it allows for a very accurate characterization of the substrate and of the adlayer morphology during the layer growth; last but not least thermal energy He has no influence whatsoever even on very unstable adlayer phases.

We will review first briefly the main experimental features of the application of He-scattering for the investigation of physisorbed rare-gas layers. Then we will illustrate with a few examples the structural richness of the rare-gas monolayers adsorbed on Pt(111). Finally, we will present the picture of the lattice dynamics of these systems.

## 2. THERMAL He-SCATTERING AS A PROBE OF ADSORBED LAYERS

The basic capabilities of He-scattering for the investigation of surface structure were already apparent in the early pioneering work in Otto Stern's laboratory in Hamburg in the thirties (ref. 4). However, it was not until the advent of the nozzle-beams that He-beams have become a highly efficient surface investigation tool. The nozzle-beam sources lead simultaneously to a dramatic increase of both the intensity and the monochromaticity of the beams, an achievement comparable only to that of the lasers for light beams. The three main approaches in He-surface scattering allow for an almost exhaustive characterization of rare gas layers: 1) diffraction - for structure (ref. 5), 2) inelastic scattering - for dynamics (ref. 6,7), 3) and diffuse elastic scattering in combination with interference - for thermodynamics, island formation, defect site occupation, degree of adlayer and substrate perfection (ref. 8-11).

A modern He surface-scattering spectrometer (see e.g. ref. 12) provides a highly monochromatic ($\Delta\lambda/\lambda \approx 0.7\%$), intense ($> 10^{19}$ He/sterrad. sec) and collimated ($\Delta\Omega \approx 10^{-6}$ sterrad) He-beam, with energies in the range 10-100 meV. The corresponding wavelength range (1.5-0.4 Å) is well suited for structure determinations which - due to the extreme sensitivity for the outermost layer - can be extended even to shallow, large period adlayer bucklings and matter waves. The resolution attained so far is of the order of 0.01 $Å^{-1}$. This is certainly inferior to X-ray performances, but - due again to the surface sensitivity - the signal/background ratio for the adlayer diffraction peaks is incomparably larger.

The narrow energy spread of the beam in conjunction with a high quality time-of-flight (TOF) system leads to an overall energy resolution for inelastic measurements of less than 0.4 meV at 18 meV beam energy. This and the relatively high cross-section for inelastic events in the range below 15-20 meV makes He-scattering an ideal instrument for the investigation of even detailed features of rare-gas layer phonons (at least of those perpendicularly polarized).

## 3. MONOLAYER STRUCTURES ON CORRUGATED SUBSTRATES

Atoms adsorbed on a periodic substrate can form ordered structures. These structures may be either in or out of registry with the structure of the substrate. It is convenient to describe this ordering by relating the Bravais lattice of the adlayer to that of the substrate surface. Park and Madden [13] have proposed a simple vectorial criterion to classify the structures. Let $\vec{a}_1$ and $\vec{a}_2$ be the basis vectors of the adsorbates and $\vec{b}_1$ and $\vec{b}_2$ those of the substrate surface; these can be related by

$$\begin{bmatrix} \vec{a}_1 \\ \vec{a}_2 \end{bmatrix} = G \begin{bmatrix} \vec{b}_1 \\ \vec{b}_2 \end{bmatrix} \qquad (1)$$

with the matrix

$$G = \begin{bmatrix} G_{11} & G_{12} \\ G_{21} & G_{22} \end{bmatrix} \qquad (2)$$

$\vec{a}_1 \times \vec{a}_2$ and $\vec{b}_1 \times \vec{b}_2$ are the unit cell areas of the adlayer and substrate surface, respectively; det G is the ratio of the two areas. The relation between the two ordered structures is classified by means of this quantity as follows:

i) det G = integer
the structure of the adlayer has the same symmetry class as that of the substrate and is in registry with the latter; the adlayer is termed commensurate.

ii) det G = irrational number
the adlayer is out of registry with the substrate; the adlayer is termed incommensurate.

iii) det G = rational number
the adlayer is again in registry with the substrate. However, whereas in i) all adlayer atoms are located in equivalent high symmetry adsorption sites, here only a fraction of adatoms is located in equivalent sites; the adlayer is termed high-order commensurate.

In Fig. 1, we show a simple one-dimensional model illustrating this classification. The periodicity of the substrate surface is represented by a sinusoidal potential of period b and the adlayer by a chain of atoms with nearest neighbor distance a.

Assuming that the structural mismatch between adlayer and substrate is not too large (< 10-15%), the nature of the adlayer ordering on the substrate is largely determined by the relative interaction strength $e_1/V_c$, where $e_1$ is the lateral adatom interaction in the layer and $V_c$, the modulation of the adsorbate-substrate potential parallel to the surface. When the diffusional barrier $V_c$ is large compared to the lateral interaction $e_1$ commensurate structures will be formed. On the other hand, when the lateral adatom interactions dominate, incommensurate structures will be favored. Only when the competing interactions are of comparable magnitude, may both registry and out of registry structures be stabilized by the complex interplay of these interactions and other parameters.

We have recently measured the energetics of the adsorption of the rare gases Ar, Kr and Xe on the Pt(111) surface by means of thermal He-scattering. In table 1, we summarize the pertinent values. From inspection of the relevant quantities in the table we can deduce that rare gas-monolayers on Pt(111) appear to be well suited to study structural 2D solid-solid transitions.

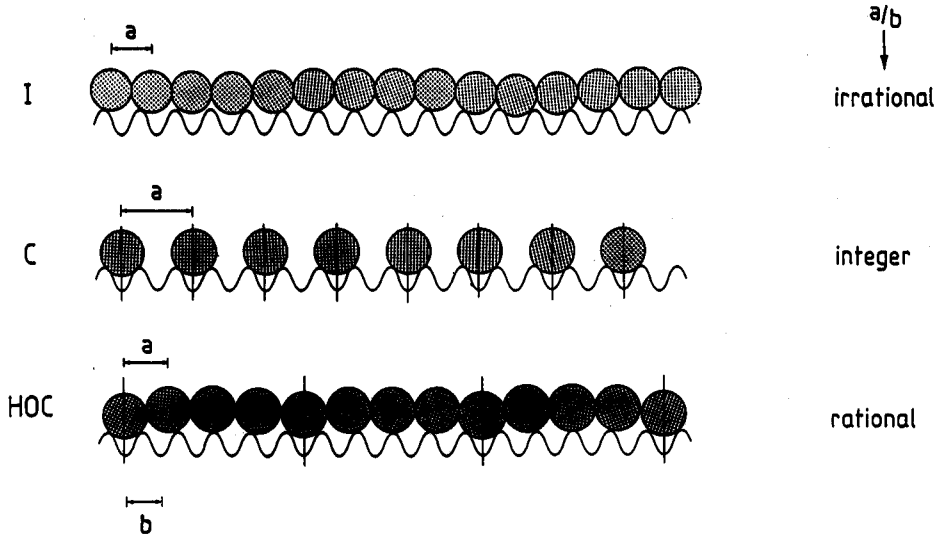


Fig. 1. One dimensional model of a physisorbed monolayer. The substrate is represented by a sinusoidal potential of period b and the adlayer by a chain of atoms with lattice constant a.

Table 1. Characteristic energies (meV) of rare gas-adsorption on Pt(111) in the monolayer range.

| | Xe | Kr | Ar |
|---|---|---|---|
| isosteric heat $q_{st}$ at $\Theta \to 0$ | 277 | 128 | 78 |
| lateral attraction $e_\ell$ | 43 | 26 | 17 |
| diffusional barrier $V_c$ | ~ 30 | ~ 10-20 | ~ 10-20 |

## 4. THE COMMENSURATE-INCOMMENSURATE (CI) TRANSITION IN 2D

Only when the lateral adatom interaction and the substrate corrugation are comparable, an ordered commensurate (C) adlayer can undergo a transition into an incommensurate (I) phase as a function of coverage or temperature. The CI-transition is driven by the formation of line defects, so called misfit dislocations as was demonstrated first by Frank and van der Merwe [14]. These authors studied a linear chain of atoms with a lattice constant a placed in a sinusoidal potential of amplitude V and periodicity b. The mutual interactions of atoms in the chain a represented by springs with a spring constant K. The calculations reveal that for slightly different lattice parameters of chain and substrate, i.e. for a weakly incommensurate adlayer, the lowest energy state is obtained for a system which consists of large commensurate domains separated by regions of bad fit. The regions of poor lattice fit are dislocations with Burgers vectors parallel to the length of the chain.

In two-dimensional systems domain walls are lines. In a triangular lattice there are three equivalent directions and therefore, domain walls

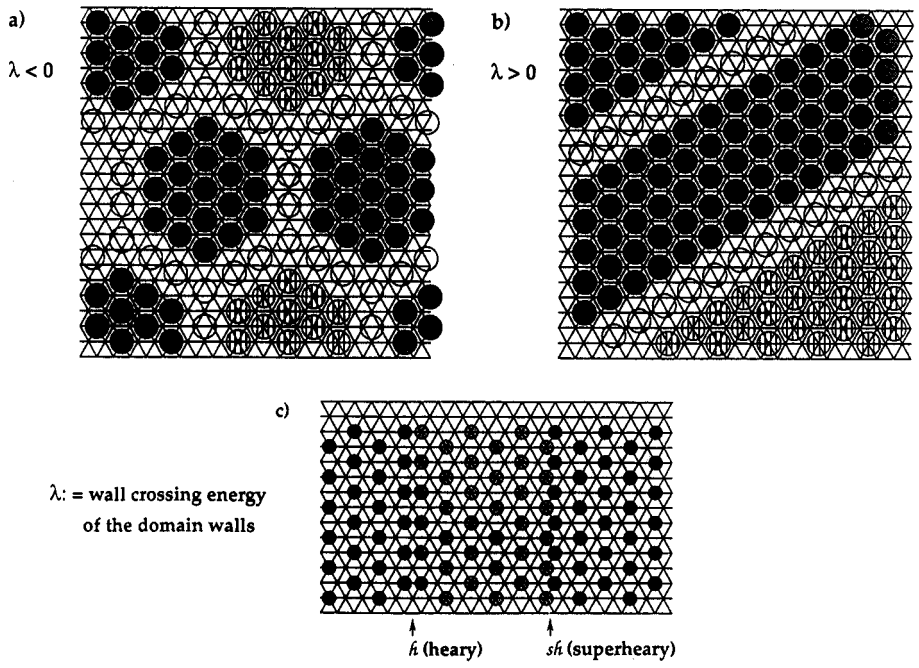


Fig. 2. Domain wall systems of an $(\sqrt{3}x\sqrt{3})$ R30° phase on a triangular substrate lattice; the walls are of the "light" type.

can cross. Using Landau theory, Bak, Mukamel, Villain and Wentowska (BMVW) [15] have shown that it is the wall crossing energy, $\Delta$, which determines the symmetry of the weakly incommensurate phase and the nature of the phase transition. For attractive walls, $\Delta < 0$, a hexagonal network of domain walls (HI) will be formed at the CI transition because the number of wall crossings has to be as large as possible. This C-HI transition is predicted to be first order. For repulsive walls, $\Delta > 0$, the number of wall crossing has to be as small as possible, i.e. a striped network of parallel walls (SI) will be formed in the incommensurate region. The C-SI transition should be continuous. The striped phase is expected to be stable only close to the CI phase boundary. At large incommensurabilities the hexagonal symmetry should be recovered in a first order SI-HI transition. In fig. 2 we summarize the possible domain wall structures. Superheavy and heavy walls are characteristic for those systems in which the incommensurate phase is more dense than the commensurate phase while for light and superlight walls the opposite holds.

The most completely studied examples of the CI-transition in 2D adlayer systems occur in the Kr monolayer on the basal (0001) plane of graphite [16] and in the Xe monolayer on the Pt(111) surface [17]. Here we will discuss briefly the physics of the Xe/Pt system. Below coverages of $\Theta_{Xe} \simeq 0.33$ (Xe adatoms per one Pt-substrate atom) and in the temperature range 60-99 K the xenon condenses in a $(\sqrt{3}x\sqrt{3})R30^{o}$ commensurate solid phase. This phase has very

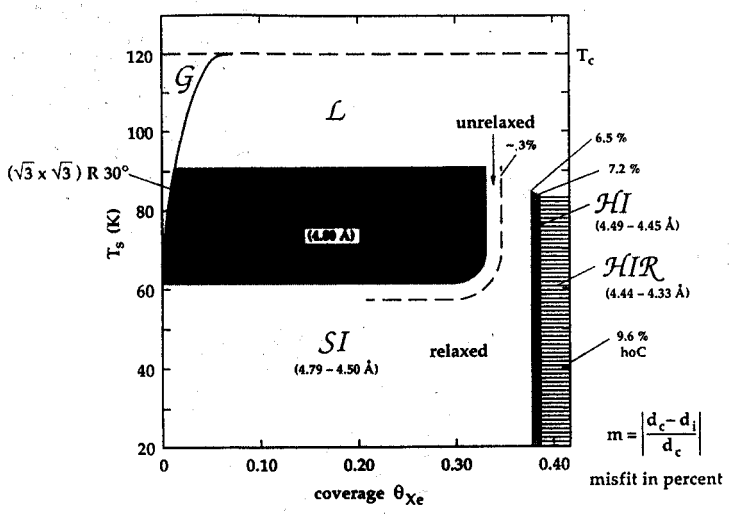


Fig. 3. Schematic phase diagram of monolayer Xe on Pt(111). C, SI, HI, HIR denote the commensurate $(\sqrt{3}x\sqrt{3})$ R30°, the striped incommensurate, the hexagonal incommensurate and the hexagonal incommensurate rotated 2D solid phases. G and L denote the 2D gas and liquid, respectively.

sharp diffraction peaks, characteristic for coherent Xe-domains which are about 800 Å in size. As the Xe-coverage is increased above 0.33 the relatively loosely packed Xe-structure undergoes a transition from the commensurate $\sqrt{3}$ structure to an incommensurate striped solid phase with superheavy walls (see fig. 2). This weakly incommensurate solid is able to accomodate more Xe atoms than the commensurate phase by dividing into regions of commensurate domains separated by a regularly spaced array of striped denser domain walls. Increasing coverage causes the commensurate domains to shrink and brings the walls closer together. The domain walls are thus a direct consequence of the system's efforts to balance the competition between the lateral Xe-Xe and the Xe-Pt interactions. The C-SI transition can also be induced by decreasing the temperature below ~ 60 K at constant coverage ($\Theta_{Xe} < 0.33$); the driving force for this temperature induced CI-transition being anharmonic effects [18].

The usual measure for the incommensurability of an I-phase is the misfit $m = (a_C - a_I)/a_C$, where $a_C$ is the lattice parameter of the commensurate phase and $a_I$ that of the incommensurate structure. For striped I-phases, the misfit has of course uniaxial character, being defined only along the direction perpendicular to the domain walls. Qantitative measurements of the misfit during the C-SI transition of Xe on Pt(111) [17] have revealed a power law of the form:

$$m = \frac{1}{\ell} \propto (1-T/T_C)^{0.51\pm0.04} \qquad (3)$$

i.e., the distance between nearest neighbor walls $\ell$ scales with the inverse square root of the reduced temperature. This square root dependence is based on entropy mediated repulsing meandering walls and is in accord with theoretical predictions [19].

With increasing incommensurability the domain wall separation becomes progressively smaller until at a critical misfit of ~ 6.5% the Xe domain wall lattice rearranges from the striped to the hexagonal symmetry (fig. 2) in a first order transition [20]. A further increase of the incommensurability by adding more and more Xe eventually results in an adlayer rotation to misalign itself with the substrate in order to minimize the increasing strain energy due to the defect concentration. This continuous transition to a rotated phase (HIR) follows a power law $\varphi \propto (m-0.072)^{1/2}$ starting at a critical separation between nearest neighbor walls $\ell_C \simeq 10$ Xe-row distances.

Novaco and McTague [21] have shown that these adlayer rotations for monolayers far from commensurability are driven by the interconversion of longitudinal stress into transverse stress. These authors also showed that the rotational epitaxy involves mass density waves (MDW) [also known as static distortion waves (SDW)], i.e. a periodic deviation of the position of monolayer atoms from their regular lattice sites. Indeed, it is the combination of rotation and small displacive distortions of the adatom net which allows the adlayer to minimize its total energy in the potential relief of the substrate. In a diffraction experiment, these mass density waves should give rise to satellite peaks.

Fuselier et al. [22] have introduced an alternative concept to explain the adlayer rotation: the "coincident site lattice." They pointed out that energetically more favorable orientations are obtained for rotated high-order commensurate structures. The larger the fraction of adatoms located in high-symmetry, energetically favorable sites, the larger the energy gain and the more effective the rotated layer is locked. It turns out that the predictions of the coincident site lattice concept for the rotation angle versus misfit agrees well with the Novaco-McTaque predictions.

The experimental results do not allow so far to decide whether the Novaco-McTague mechanism involving MDW or the "coincident in lattice" concept involving HOC structures, or even both have the determining role in driving the adlayer rotation. In particular, no mass density wave satellities have been observed in electron and x-ray diffraction experiments from rotated monolayers [23] so far. In He diffraction scans of rotated Xe monolayers on Pt(111) we have, however, observed satellite peaks at small Q-vectors. Originally we assigned these peaks to a higher-order commensurate superstructure [8]. However, Gordon [24] pointed out that these satellites could be due to the MDW. Recently we have shown that both MDW as well as high-order commensurate buckling satellites are present in the rotated Xe monolayers on Pt(111)[2]; the arguments are recalled in the following three paragraphs. The distinction between the two types of satellites is straightforward. As pointed out by Gordon, the wave vector, Q, of the MDW satellites should be subject to the following relation:

$$Q \simeq (8\pi/a^{R}_{Xe})\ (m/\sqrt{3})\ (1+m/8), \qquad (4)$$

with m the misfit, and $a^{R}_{Xe}$ the lattice of the rotated Xe layer. For not too large misfits, this MDW satellite should appear in the same direction as

the principal reciprocal lattice vector of the Xe layer, i.e., in the $\bar{\Gamma}\,\bar{M}_{Xe}$ direction. On the other hand, according to its particular structure (Fig. 3, Ref. 8), the commensurate buckling should have its maximum amplitude in the $\bar{\Gamma}\,\bar{K}_{Xe}$ direction. Moreover, these commensurate buckling satellites should only be present at the particular coverages where a certain high-order commensurability becomes favorable, in the present case at monolayer completion (m=9.6%) (see also ref. 25), whereas the MDW satellites should be present in the entire misfit range where the Xe layer is rotated (7.2%-9.6%).

In fig. 4 we show the dispersion of the MDW-satellites deduced from a series of diffraction scans, taken in the $\bar{\Gamma}\,\bar{M}_{Xe}$-direction, and compare them with Gordon's prediction for the MDW given above. The data follow qualitatively the predicted dependency; the agreement becomes quantitatively at misfits > 8%. The reason for the better agreement at large misfits is due to the fact that Gordons analysis of the MDW (similar to Novaco-MacTague's model calculations) have been performed in the linear response approximation of the adsorbate-substrate interaction; this approximation is only justified at large misfits, where the adlayer topography corresponds rather to a weakly modulated uniform layer than to a domain wall lattice [26].

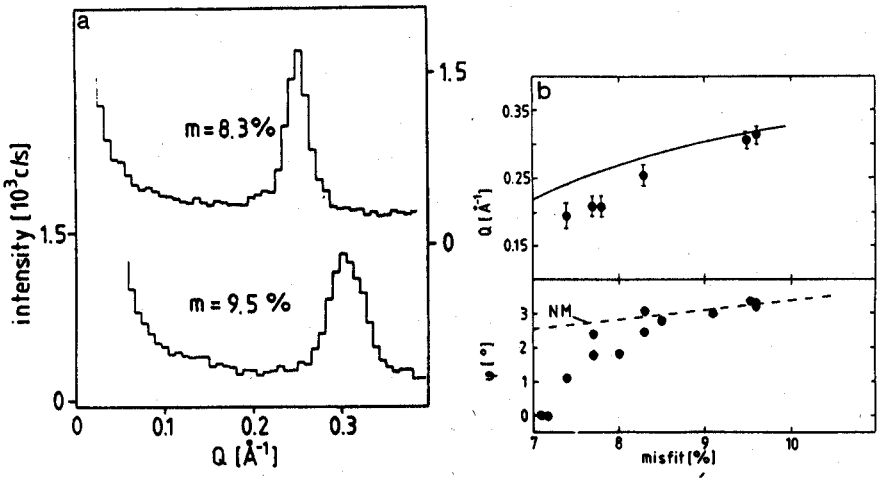


Fig. 4. a) Polar He diffraction scans of rotated Xe monolayers on Pt(111) taken along the $\bar{\Gamma}\bar{M}_{Xe}$ azimuth at misfits of 8.3% and 9.5%.
b) Dispersion of the mass density wave sattelites with misfit m. The solid line is Gordon's relation.

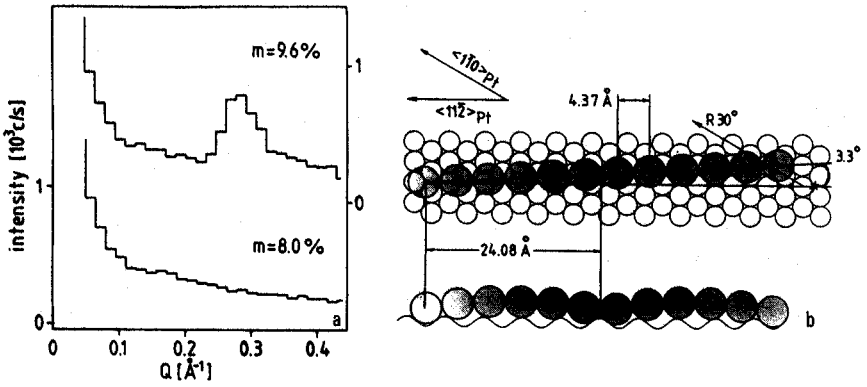


Fig. 5. a) Polar He-diffraction scans of rotated Xe monolayers on Pt(111) taken along the $\bar{\Gamma}\bar{K}_{Xe}$ azimuth at misfits 8% and 9.6%.
b) Upper and side view of a 3.3° rotated domain at m = 9.6%.

In Fig. 5 we show scans like in Fig. 4 but now measured in the $\bar{\Gamma}\,\bar{K}_{Xe}$ direction at small Q for rotated Xe layers of misfit 8% and 9.6%. At variance with the scans in the $\bar{\Gamma}\,\bar{M}_{Xe}$ direction (fig. 4), a satellite peak is observed only for the complete Xe monolayer (m=9.6%). Being present only at a particular misfit this peak does not originate from a MDW but from the buckling of a HOC-structure. The location of this satellite peak at Q = 0.28 $Å^{-1}$ corresponds to a buckling period of 23 Å and can be ascribed to a high-order commensurate structure shown in fig. 5b and described in detail in ref. 8.

## 5. THE SUBSTRATE CORRUGATION OF CLOSE PACKED METAL SURFACES

The discovery of the existence of various solid Xe phases on Pt(111) was actually a surprise because the hexagonal close packed Pt(111) surface was considered essentially non corrugated. As already stated in the introduction, the various solid phases of adsorbed monolayers arise as a result of competing interactions; lateral adatom interaction versus the corrugation of the holding potential. In particular the commensurate $\sqrt{3}$ phase was unexpected; at 60 K the "natural" two-dimensional Xe-lattice parameter in the absence of any substrate would be about 8% smaller than the $\sqrt{3}$ distance of the Pt substrate (4.80 Å). In order to stabilize the commensurate Xe-phase the corrugation of the substrate has to compensate this substantial strain and to counterbalance the attractive lateral Xe-interaction, which is $e_\ell^{Xe-Xe/Pt}$ = 43 meV per atom.

It is indeed still a widespread belief that for rare gases adsorbed on close packed metal surfaces the lateral corrugation is negligible. This belief

originates in the very low corrugation of the interaction potential as deduced from He-diffraction data. This argument, although found often in literature, is wrong and thus misleading. From small corrugations deduced from He-diffraction experiments it can not be inferred, that the lateral corrugation felt by **all** rare gases adsorbed on close packed metal surfaces is likewise small.

First, in diffraction experiments the He-atoms probe the corrugation of the repulsive interaction potential in the region of positive energies, while adsorbed atoms feel the corrugation of the bottom of the attractive potential well, i.e. corrugations at two different locations on the potential curve. Second, and this is even more important, the interaction of the heavier rare gases Xe, Kr, Ar or even Ne differs appreciably from the interaction of He with the same substrate (e.g. the binding energy for He and Xe on Pt(111) are about 5 meV and 311 meV respectively!).

It has been shown by Steele (27), that the physisorption potential of rare gas atoms on a crystal surface, is represented, in a good approximation, by a Fourier expansion in the reciprocal lattice vectors G of the substrate surface

$$V(r,z) = V_0(z) + V_{mod}(r) = V_0(z) + \sum_G V_G(z) \exp(iGr) \quad (5)$$

evidencing nicely the lateral modulation of the adsorption energy. Here $z$ ($> 0$) is the distance of the adatom perpendicular to the surface and $r$ the coordinate parallel to the surface. $V_0(z)$ is the mean potential energy of an adatom at a distance $z$, $V_G$ the principal Fourier amplitude. Owing to the rapid convergence of the Fourier series, the second term is usually already one order of magnitude smaller than the first order term, and for the basal plane of graphite Gr(0001) and the fcc(111) surface we obtain:

$$V(\vec{r}) = V_0(z) \mp V_G \{\cos(2\pi s_1) + \cos(2\pi s_2) + \cos 2\pi(s_1+s_2)\} \quad (6)$$

respectively. Here $s_1$ and $s_2$ are the dimensionless coordinates of the atoms in the substrate surface unit cell.

If we assume a 12-6 Lennard-Jones pair potential to represent the interaction between various atoms of the adsorbate/substrate system, the corrugation in the unit cell of a particular surface is entirely determined by the ratio $\sigma/a$, by the magnitude of the binding energy $V_0$ and by the sign of $V_G$, with $\sigma$ being the Lennard-Jones diameter of the adatom and a being the nearest neighbor distance in the substrate surface.

The location of the energetically most favorable adsorption site is determined by the sign of $V_G$. For $V_G > 0$, the energy minima on a fcc(111) surface are at three fold hollow sites (H) and the barrier of diffusion across the bridge sites (B) is given by $V_C = V_{H-B} = V_G$. For $V_G < 0$, on the other hand, the energy minima are at on top sites (T) and the barrier of diffusion $V_C = V_{T-B} = -8\ V_G$. From intuition it was always believed that the sign of the Fourier amplitude has to be positive, i.e., the preferred adsorption site of the rare gas atom would be the threefold hollow sites. In this picture the energy difference between adsorption of a Xe-atom in a hollow and in a bridge position, $V_{H-B}$, amounts to about $\sim 0.01\ V_o$ ( $\approx$ 3 meV) for the (111) surface of Pt.

A detailed analysis of the diffraction patterns in the striped incommensurate phase of Xe/Pt(111) by Gottlieb [28] came to the remarkable conclusion that the preferred adsorption sites of the Xe atoms are on top of platinum atoms rather than in threefold hollow sites, i.e. the sign of $V_G$ is negative. From his analysis he deduced the values $V_C = V_{T-B} = -V_G \approx 6\text{-}8$ meV for the Xe/Pt(111) system.

The Lennard-Jones potential is only a crude approximation of the interaction between a rare gas atom and a metal surface. Drakova et al. [29] demonstrated recently in a self consistent Hartree-Fock calculation, that the corrugation of the rare gas - transition metal surface potential is substantially enhanced by the hybridization between occupied rare gas orbitals and empty metal d-orbitals which particularly in the case of transition metal elements like Pd or Pt gives a strong increase of the corrugation.

The corrugation enhancement due to orbital hybridization as well as the negative sign of the Fourier amplitude $V_G$ has been demonstrated by Müller [30] in a very recent ab initio cluster calculation. The Pt(111) surface was modelled by a $Pt_{22}$ cluster. The total energy of the Xe-$Pt_{22}$ system was calculated in the Kohn-Sham scheme with the local-density approximation for exchange and correlation, and a localized muffin-tin orbital basis including s,p and d orbitals in all metal sites. In his ab-intio calculations Müller finds the on top position of Xe as the energetically most favorable location with a binding energy of 307 meV. The corrugation is determined to be $V_C = V_{T-B} \approx 22$ meV.

This large corrugation is consistent with experimental data of Kern et al. [31] estimated the corrugation of the Xe/Pt(111) system to about 10% of the binding energy which is ~ 30 meV. A value which is compatible with the value of

the diffusion barrier of Xe on W(110) (also a rather close packed surface) which has been measured to 47 meV [32]. It is thus no more a surprise but a logical consequence that Xe on Pt(111) can form a commensurate $\sqrt{3}$-phase.

## 6. HIGH ORDER COMMENSURATE PHASES

Another interesting concept describing structural phase transitions of adsorbed layers has been developed by Aubry [33]. The basic idea is that any adlayer structure incommensurate with the substrate can be approximated within any given accuracy by a so called high-order commensurate (HOC) structure. These HOC structures are characterized by a (large) commensurate unit cell hosted by several adlayer atoms. Since a fraction of the adatoms will always lock into preferential adsorption sites these HOC (locked) phases should be energetically favoured with respect to a true incommensurate (floating) phase. If the corrugation potential is sufficiently large, it is expected that the phase diagram of the adlayer is composed of several HOC phases. The corresponding (first order) phase transitions will involve discrete jumps of the interatomic distance moving from one HOC phase to the other. Such a stepwise variation of the lattice parameter within a series of HOC phases is called a "devil's staircase". Of course, this simple picture is modified at elevated surface temperature when thermal fluctuations become important and can destabilize these HOC phases with large unit cells.

It is generally accepted that on the same substrate the absolute magnitude of the corrugation increases with the size of the rare gas adatom, while the corrugation energy decreases relative to the binding energy of the adatom as well as relative to the lateral adatom interaction [34]. Thus, within our simple model of competing interactions (corrugation versus lateral attraction) we expect on the Pt(111) surface a gradual transition from the floating Xe monolayer with its rich diversity of incommensurate domain wall phases to locked Kr or Ar layers which are dominated by the lock-in forces of the substrate, favoring HOC-phases instead of incommensurate domain wall phases.

Until very recently, there has been no convincing experimental evidence for the existence of high order commensurate physisorbed layers. This appeared to support the widespread belief that "experimentally it is impossible to distinguish between a high order-C structure and an incommensurate structure". This belief is certainly legitimate, if the only accessible experimental information is the ratio of the adlayer and substrate lattice basis vectors. Indeed, because one can find always one rational number within the confidence range of any experimental irational number, i.e. the basis vectors supplied by

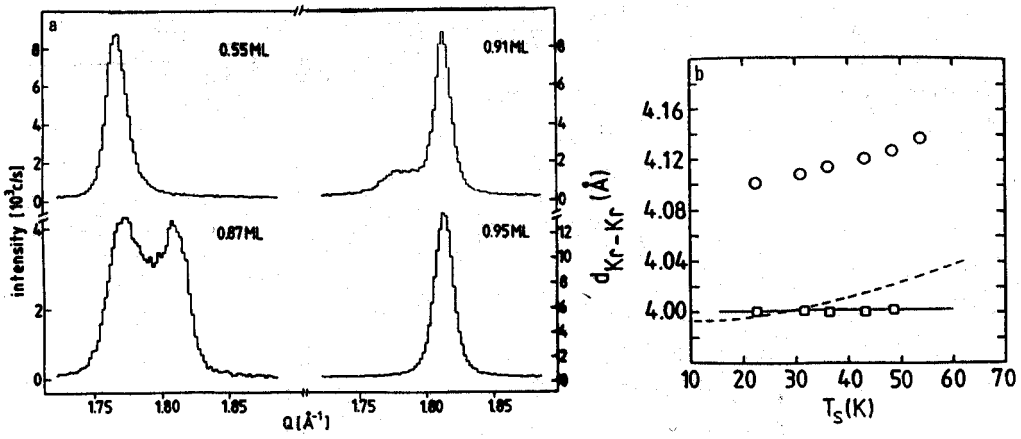


Fig. 6. a) Polar He-diffraction scans of the $(1,0)_{Kr}$-diffraction order from Kr adlayers on Pt(111) at various Kr submonolayer coverages at $T_S$=25 K. b) Kr-layer lattice spacing vs $T_S$ for the ( ) high (0.95 ML) and (o) low (0.5 ML) coverage phase; temperature dependence of the lattice spacing of (---) Pt-substrate, and of ( - - -) bulk Kr.

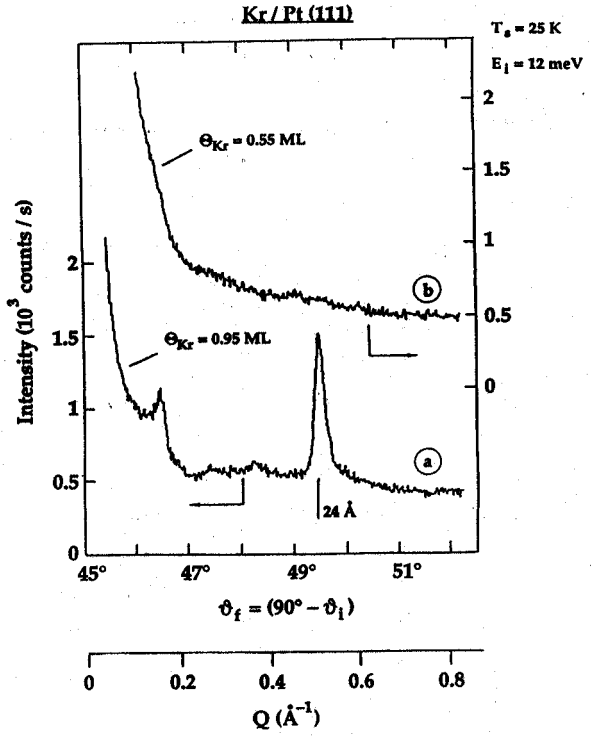


Fig. 7. Polar He diffraction scans of Kr monolayers in the vicinity of the specular peak ($Q = 0\text{Å}^{-1}$); i) high (0.95 ML) and ii) low (0.5 ML) coverage phse, taken along the $\bar{\Gamma}\bar{K}_{Kr}$ -azimuth.

the most refined experiment are always compatible with a high (enough) order commensurate phase. There are, however, two other experimentally accessible parameters which allow a unequivocal distinction between a high order commensurate "locked" and an incommensurate "floating" layer. First: the superstructure formed by the atoms located in equivalent, high symmetry sites. These stronger bound atoms being located "deeper" in the surface than the others, the adlayer is periodically buckled. Because of the extreme sensitivity of He-scattering to the surface topography, this superstructure, which characterizes high order commensurate layers, is directly accessible to high resolution He-diffraction experiments. Second: the thermal expansion. Indeed, a "floating" layer is expected to thermally expand very much like the corresponding rare gas bulk crystal, while a "locked" layer has to follow by definition the substrate at which it is locked. The thermal expansion of rare gas solids being at least ten times larger than that of substrates normally employed, the destinction between high order commensurate "locked" and incommensurate "floating" becomes straightforward. This very sharp criterion requires that the "locking" is strong enough to withstand temperature variations over a sufficiently large range ($\geq$ 10 K) to allow for reliable thermal expansion measurements.

Figure 6a) shows a series of polar He-scans of the $(1,1)_{Kr}$ diffraction peak taken at 25 K along the $\bar{\Gamma}\bar{M}_{Kr}$ direction of the Kr monolayers adsorbed on a Pt(111) surface at coverages between 0.5 and 0.95 ML [25]. The sequence is characteristic for a first order phase transition from a hexagonal solid phase — with wavevector Q = 1.769 $\mathring{A}^{-1}$ ($d_{Kr}$ = 4.10$\mathring{A}$) to one with Q = 1.814 $\mathring{A}^{-1}$ ($d_{Kr}$ = 4.00 $\mathring{A}$), below and above 0.8 ML, respectively. During the phase transition the intensity diffracted from one phase increases at the expense of the other.

The question concerning the incommensurate "floating" versus high order commensurate "locked" nature of the two Kr-phases has been adressed by looking at their thermal expansion behavior and by searching for superstructure satellites. In fig. 6b) the measured Kr-Kr interatomic spacing versus temperature is shown for submonolayer films of coverage 0.5 ML and 0.95 ML. The difference is striking. The low coverage phase shows a variation with temperature very much like bulk Kr (dashed) and is thus an incommensurate "floating" phase. On the contrary, the lattice parameter of the high coverage phase is - that of the Pt substrate (solid) - constant within experimental error in the same temperature interval; accordingly, this Kr-phase is high order commensurate "locked".

This assignment is supported by inspection of fig. 7, where polar scans (He-beam energy 12 meV) in the $\bar{\Gamma}\bar{K}_{Kr}$ -direction of the "floating" and of the

"locked" Kr-layer are shown. The scans differ substantially: the locked scan clearly evidences the presence of a superstructure, while the floating one does not. The superstructure peak at Q = 0.532 ± 0.022 $\AA^{-1}$ corresponds to 1/5 of the Pt-substrate principal lattice vector, i.e. the Kr-layer forms a (5x5)R0° HOC phase.

In contrast to Kr, Ar adsorbs on the clean Pt(111) surface in a hexagonal solid phase aligned with respect to the substrate[42]. In the submonolayer regime

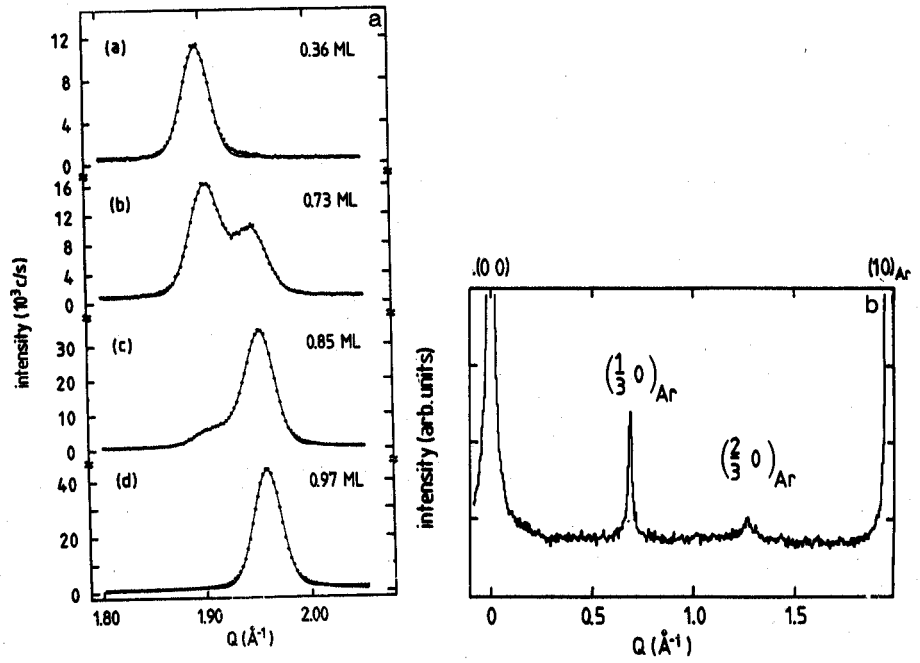


Fig. 8. a) Polar He diffraction scans of the $(1,0)_{Ar}$ -diffraction order for different Ar coverages b) Polar He diffraction scan of the high coverage ($\Theta$ = 0.91 ML) Ar monolayer on Pt(111) in an extended Q-range.

a structural phase transition of the physisorbed Ar layer occurs at a coverage $\Theta \simeq 0.75$ ($\Theta$ = 1 refering here to full monolayer coverage): At lower coverage ($\Theta < 0.6$) the first order diffraction peak of the Ar-phase is centered at Q = 1.90 $\AA^{-1}$, corresponding to a lattice parameter a = 3.81 Å. Upon increase of the Ar coverage a second first order diffraction peak at Q = 1.96 $\AA^{-1}$ emerges,

corresponding to an Ar-phase with lattice parameter a = 3.70 Å, i.e. slightly compressed with respect to the first. While the intensity of the first peak continuously decrease upon further Ar-adsorption, the second peak at Q = 1.96 $Å^{-1}$ becomes more intense. At $\Theta \simeq 0.75$ the two diffraction peaks have about equal intensities while above $\Theta \geq 0.9$ the first peak has vanished and only the second one is observed. The discontinuous change of the diffraction peak position and the observed phase coexistence indicate that this phase transition is of first order.

The Ar phase at higher coverage shows no significant thermal expansion in contrast to the large expansion of bulk Ar, indicating that the adlayer is a locked commensurate phase. In addition, superstructure peaks are observed in this high coverage phase at 1/3 and 2/3 of the wave-vector position of the first order Ar diffraction peak (fig. 8b). Thus the period of the commensurate unit cell equals three interatomic Ar distances (~ 11 Å). From the known lattice parameter of the Pt(111) substrate $a_{Pt}$ = 2.77 Å it follows that the Ar phase at higher coverage ($\Theta \geq 0.75$) is a $(4x4)R0^{o}$ HOC-phase with a commensurate unit cell of length $3xa_{Ar} = 4 \times a_{Pt}$ = 11.08 Å. The analysis of the low coverage phase is more difficult. Although further investigation is needed for a final

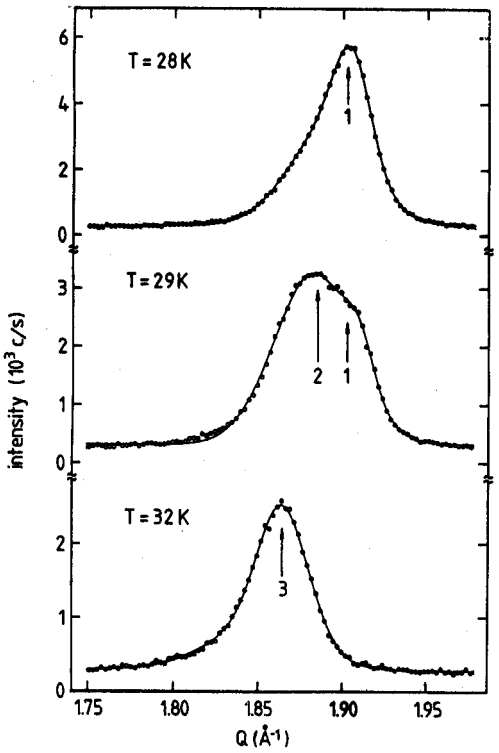


Fig. 9. Polar He-diffraction profiles of the $(1,0)_{Ar}$ peak in the low Ar coverage regime ($\Theta$ = 0.36 ML) at different surface temperatures.

conclusion, our experimental data indicate that also the low coverage Ar phase ($\Theta \lesssim 0.75$) is partially locked. The low coverage Ar phase ($\Theta_{Ar} \approx 0.36$ ML) was prepared by dosing Ar at low surface temperature (~ 20 K) and successively briefly annealing the adlayer. Depending on the annealing temperature and the annealing time either an Ar lattice parameter of $a_{Ar} \simeq 3.81$ Å (1) or a slightly larger value of $a_{Ar} \simeq 3.83$ Å (2) was obtained.

The fact that there are indeed discrete jumps in the Ar lattice parameter as expected for a transition between phases in registry with the substrate is demonstrated in fig. 9. Here the polar diffraction profiles recorded from an Ar adlayer in the low coverage phase ($\Theta = 0.36$ ML) for different surface temperature are shown. The three spectra (a)-(c) indicate the coexistence and the discontinuous transition between (partially) locked structures; they are characterized by the lattice parameters $a_{Ar} \simeq 3.81$ Å ($a_{Ar}/a_{Pt} = 11/8$), $a_{Ar} \simeq 3.84$ Å ($a_{Ar}/a_{Pt} = 18/13$) and $a_{Ar} \simeq 3.88$ Å ($a_{Ar}/a_{Pt} = 7/5$).

## 6. MONOLAYER FILMS AND DYNAMICS OF COMPETING INTERACTIONS

When adsorbing a layer of atoms (for example rare gas atoms) on a substrate surface we are not dealing only with static interaction effects which determine the structure of the adlayer but also with dynamical interactions between collective excitations (for example phonons) of adlayer and substrate.

The phonon spectrum of a crystal surface consists of two parts (fig. 10): The bulk bands, which are due to the projection of bulk phonons onto the two-dimensional Brillouine zone of the particular surface, and the specific surface phonon branches [7]. A surface phonon is defined as a localized vibrational excitation with an amplitude which has wavelike characteristics parallel to the surface and decays exponentially into the bulk, perpendicular to the surface. Of particular interest is the lowest frequency mode below the transverse bulk band edge. In this mode, the atoms are preferentially vibrating in the plane defined by the surface normal and the propagation direction, i.e. in the sagittal plane. This wave is the famous Rayleigh wave.

Adsorbing a layer of densely packed atoms on the substrate surface adds three additional phonon modes to the system; two in-plane modes and one mode with polarization perpendicular to the surface. The frequency and dispersion of these modes is governed by the "spring constants" which couple the adatoms laterally and to the substrate. In the following we concentrate on the perpendicular mode. In physisorbed systems, the electronic ground state of the adsorbate is only weakly perturbed upon adsorption. The physisorption potential

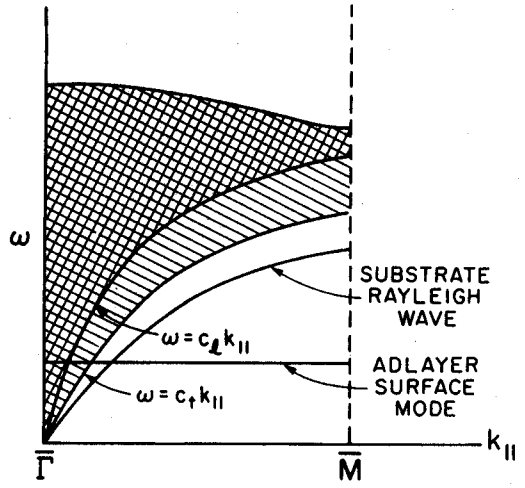


Fig. 10. Schematic normal mode spectrum of a rare gas monolayer physisorbed on a single crystal surface [36].

is rather flat and shallow, i.e. the spring constant of the vertical adatom-motion is weak and the corresponding phonon frequencies are low compared to the substrate Rayleigh wave at the zone boundary.

The first systematic theoretical and experimental exploration of the dynamics of rare gas monolayers on metal surfaces has been performed on Ag(111) [35,36]. The lattice dynamical calculations were based on a simple model - Barker pair potentials - to account for the lateral adatom interactions and a rigid holding substrate. The calculations have supplied dispersion curves fully adequate to account for the available experimental data.

As expected from any model involving only central forces between adatoms and a rigid substrate, the three modes of the monolayer decouple, and the perpendicular mode is dispersionless, i.e. the motion of the adatoms perpendicular to the surface acts like an Einstein oscillator. Because the perpendicular surface atom motions dominate the inelastic He cross sections, this dispersionless mode has been, indeed, observed in the experiment [8,35].

It is noteworthy that the most general conclusion, emerging from this first systematic exploration, has been that "coupling between adatom and substrate atom motions is potentially more important than modest variations in the nature of the adatom - adatom potential" [35]. Consistently, Hall, Mills and

Black continued their exploration by allowing now the substrate atoms to move and by focussing on the coupling between the substrate and adlayer modes [36]. The results of the calculations show that while near the zone boundary, where the substrate phonon frequencies are well above those of the adlayer, the influence of the substrate adlayer coupling is small. Near the zone center $\bar{\Gamma}$, significant anomalies introduced by the coupling are expected. These are twofold:

1) A dramatic hybridization splitting around the crossing between the dispersionless adlayer mode and the substrate Rayleigh wave (and a less dramatic one around the crossing with the $\omega = c_{\ell} Q_{\parallel}$ line - due to the Van Hove singularity in the projected bulk phonon density of states); 2) A substantial line-width broadening of the adlayer modes in the whole region near $\bar{\Gamma}$ where they overlap the bulk phonon bands of the substrate: the excited adlayer modes may decay by emitting phonons into the substrate, they become leaky modes. These anomalies were expected to extend up to trilayers even if more pronounced for bi- and in particular for monolayers. More recent experimental data of Gibson and Sibener [37] confirm qualitatively these predictions at least for monolayers. The phonon line-widths appear to be broadened around $\bar{\Gamma}$ up to half of the Brillouin zone. The hybridization splitting could not be resolved, but an increase of the inelastic transition probability centered around the crossing with the Rayleigh wave and extending up to 3/4 of the zone has been observed and attributed to a resonance between the adatom and substrate modes.

Recent measurements performed on Ar, Kr and Xe-layer on Pt(111) [38-40] with a substantially higher energy resolution ($\Delta E \leq 0.4$ meV) have now confirmed in every detail the theoretical predictions on the coupling effects.

A series of He energy loss spectra taken from a full Ar-monolayer on Pt(111) at different scattering angles are plotted over an energy-loss range from -2 to -6 meV in fig. 11. In these spectra the various features of the dynamical coupling between the adlayer and Pt substrate can be distinguished. As a reference, spectrum (d) taken at $\vartheta_i = 35^{\circ}$ corresponds to the creation of an Ar monolayer phonon with wave vector $Q = 0.78$ Å$^{-1}$, i.e., close to the edge of the 2D Ar Brillouin zone [$Q(\bar{M}) = 0.98$ Å$^{-1}$]. Since at these large Q values the Pt Rayleigh wave and the Pt bulk phonons have much higher energies than the Ar adlayer mode, no coupling of the Ar phonons to the Pt substrate is expected. Indeed, the small linewidth $\Delta E = 0.32$ meV of the Ar loss peak at -4.8 meV is determined only by the instrumental resolution $\Delta E_{instr}$ of the spectrometer without any measurable additional broadening. Spectrum (a) exhibits two-phonon loss peaks. The feature at -2.9 meV is a signature of the Pt Rayleigh wave

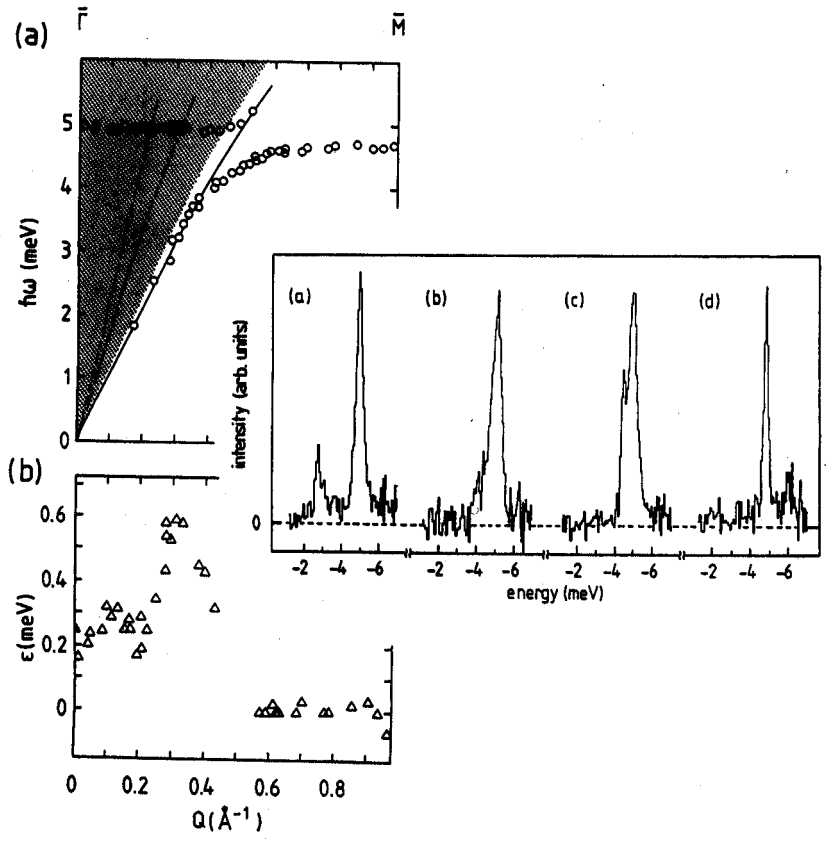


Fig. 11. Experimental dispersion curves from a monolayer Ar on Pt(111) (perpendicular polarized mode) and He TOF spectra (inset) taken at different incident angles $\vartheta$; along the $\bar{\Gamma}\bar{M}$ direction of the Ar unit cell: (a) 40.4°, (b) 38.5°, (c) 37.7°, (d) 35°. The energy of the primary He-beam was 18.3 meV.

dynamically coupled to the Ar adlayer mode. Furthermore, the Ar loss at -5.0 meV is much broader ($\Delta E \simeq 0.41$ meV) than in spectrum (d). This difference is due to the fact that the Ar phonon in (a) is created at the center of the Brillouin zone $\bar{\Gamma}(Q=0.0\ \text{Å}^{-1})$ where an effective damping of the Ar phonons due to the coupling to the projected bulk phonon bands of the Pt substrate occurs. This so called "radiative damping" of the adlayer phonon results in a linewidth broadening $\epsilon \equiv [(\Delta E)^2-(\Delta E_{instr})^2]^{1/2}$ of 0.2-0.3 meV. It is instructive to estimate the corresponding lifetime shortening due to this radiative damping. Using the Heisenberg uncertainty principle $\epsilon\Delta t = h$ the lifetime becomes $\Delta t \sim 3\times10^{-12}$s. Relating this value to the time scale of the Ar-Pt vibration ($h\omega$ = 5.0 meV, i.e., $\nu$ = 1.2 THz), a mean phonon lifetime of about three vibrational periods is obtained. Besides the radiative damping also the hybridization of the Ar adlayer mode and the Pt Rayleigh wave is observed experimentally. This is shown in spectrum (c) of Fig. 11. At these scattering conditions ($\vartheta = 37.7^{o}$) corresponding to a wave vector $Q=0.45\ \text{Å}^{-1}$ of the Ar phonon the crossing of the adlayer mode and the Pt Rayleigh wave should occur. Instead, due to the hybridization of the two modes this crossing is avoided and a phonon doublet with an energy splitting of ~ 0.8 meV is observed (note also the similar heights of the two peaks). The additional line width-broadening in the wavevector range Q=0.25 and 0.35 Å which is apparent in spectrum (b) of fig. 11 (compare with spectrum (a) and (d)) is not an artifact but can be attributed to the coupling with the projected bulk phonon band edge; the "van Hove anomaly".

More details of the dynamical coupling between an adsorbed layer and the substrate and of the phonon spectrum of thin physisorbed films (1-25 monolayers) can be found in Ref. 38-41.

REFERENCES


1. Sinha, S.K. (Ed.), Ordering in Two Dimensions (North Holland, Amsterdam, 1980)
2. K. Kern and G. Comsa, in "Chemistry and Physics of Solid Surfaces VII", ed. by R. Vanselow and R.F. Howe, (Springer, Heidelberg, 1988), p. 65
3. R.J. Birgenau and P.M. Horn; Science 232, 329 (1986)
4. I. Estermann and O. Stern; Z. Phys. 61, 95 (1930)
5. T. Engel, K.H. Rieder: Structural Studies of Surfaces with Atomic and Molecular Beam Diffraction, Springer Tracts Mod. Phys., Vol. 91 (Springer, Berlin, Heidelberg 1982)
6. J.P. Toennies: J. Vac. Sci. Technol. A 2, 1055 (1984)
7. K. Kern and G. Comsa; Adv. Chem. Phys. 76, 211 (1989)
8. K. Kern, R. David, R.L. Palmer, G. Comsa: Phys. Rev. Lett. 56, 2823 (1986)
9. A.M. Lahee, J.R. Manson, J.P. Toennies, Ch. Wöll: Phys. Rev. Lett. 57, 471 (1986)
10. J.W. Frenken, J.P. Toennies, and Ch. Wöll; Phys. Rev. Lett. 60, 1727 (1988)
11. G. Comsa, B. Poelsema, Appl. Phys. A 38, 153 (1985)
12. R. David, K. Kern, P. Zeppenfeld, G. Comsa: Rev. Sci. Instr. 57, 2771 (1986)

13. R.L. Park and H.H. Madden; Surf. Sci. 11, 188 (1968)
14. F.C. Frank, J.H. van der Merwe; Proc. Roy. Soc. A 198, 216 (1949)
15. P. Bak, D. Mukamel, J. Villain, K. Wentowska; Phys. Rev. B 19, 1610 (1979)
16. E.D. Specht, A. Mak, C. Peters, M. Sutton, R.J. Birgeneau, K.L. D'Amico, D.E. Moncton, S.E. Nagler, P.M. Horn; Z. Phys. B 69, 347 (1987) S.C. Fain, M.D. Chinn, R.D. Diehl; Phys. Rev. B 21, 4170 (1980)
17. K. Kern, R. David, P. Zeppenfeld, R.L. Palmer, G. Comsa; Solid State Comm. 62, 361 (1987)
18. M.B. Gordon, J. Villain; J. Phys. C18, 391 (1985)
19. V.L. Pokrovsky, A.L. Talapov; Sov. Phys. JETP 51, 134 (1980)
20. K. Kern; Phys. Rev. B35, 8265 (1987)
21. A.D. Novaco and J.P. McTague; Phys. Rev. B 19, 5299 (1979)
22. C.R. Fuselier, J.C. Raich and N.S. Gillis; Surf. Sci. 667 (1980)
23. C.G. Shaw, S.C. Fain and M.D. Chinn; Phys. Rev. Lett. 41, 955 (1978) K.L. D'Amico et al.; Phys. Rev. Lett. 53, 2250 (1984)
24. M.B. Gordon; Phys. Rev. Lett. 57, 2094 (1986)
25. K. Kern, P. Zeppenfeld, R. David and G. Comsa; Phys. Rev. Lett. 59, 79 (1987)
26. H. Shiba; J. Phys. Soc. Jpn. 48, 211 (1980)
27. W. Steele; Surf. Sci. 36, 317 (1973)
28. J.M. Gottlieb, to be published
29. D. Drakova, G. Doyen, and F. v. Trentini; Phys. Rev. B 32, 6399 (1985)
30. J.E. Müller; Phys. Rev. Lett. 65, 3021 (1990)
31. K. Kern, R. David, P. Zeppenfeld, G. Comsa; Surf. Sci. 195, 353 (1988)
32. J.R. Chen and R. Gomer; Surf. Sci. 94, 456 (1980)
33. S. Aubry; in "Solitons and Condensed Matter Physics", (Springer, Heidelberg, 1978), p. 264
34. G. Vidali and M.W. Cole; Phys. Rev. B29, 6736 (1984)
35. K.D. Gibson, S.J. Sibener, B.M. Hall, D.L. Mills, and J.E. Black; J. Chem. Phys. 83, 4256 (1985)
36. B.M. Hall, D.L. Mills, and J.E. Black; Phys. Rev. B32, 4932 (1985)
37. K.D. Gibson and S.J. Sibener; Faraday Discuss. Chem. Soc. 80, 203 (1985)
38. K. Kern, P. Zeppenfeld, R. David, and G. Comsa; Phys. Rev. B 35, 886 (1987)
39. B. Hall, D.L. Mills, P. Zeppenfeld, K. Kern, U. Becher, and G. Comsa; Phys. Rev. B 40, 6326 (1989)
40. P. Zeppenfeld, U. Becher, K. Kern, R. David, and G. Comsa; Phys. Rev. B 41, 8549 (1990)
41. K. Kern, U. Becher, P. Zeppenfeld, B. Hall, and D.L. Mills; Chem. Phys. Lett. 167, 362 (1990)
42. P. Zeppenfeld, U. Becher, K. Kern, G. Comsa; to be published